Scientific paper

Synthesis of Zinc Hydroxide Nanocrystals and Application as a New Electrochemical Sensor for Determination of Selected Sympathomimetic Drugs

Lotf Ali Saghatforoush,[1,*] Robabeh Mehdizadeh,[1] Soheila Sanati[1] and Mohammad Hasanzadeh[2,*]

[1] *Department of Chemistry, Payam Noor University, Tehran, I.R. of Iran*

[2] *Drug Applied Research Center, Tabriz University of Medical Sciences, Tabriz, Iran*

* *Corresponding author: E-mail: mhmmd_hasanzadeh@yahoo.com, Saghatforoush@gmail.com*

Received: 29-03-2012

Abstract

Zinc hydroxide ($Zn(OH)_2$) nanoparticles with nanocrystal morphology and grain size ~48 nm have been successfully synthesized by using a two-step, template- and surfactant-free method. The synthesized product was characterized by FTIR, powder X-ray diffraction (XRD), scanning electron microscopy (SEM), transmission electron microscopy (TEM), and energy-dispersive spectroscopy (EDX). The XRD pattern of zinc oxide confirms formation of the wurtzite structure of $Zn(OH)_2$. For the first time zinc oxide nanostructures have been used for electrocatalytic oxidation and determination of sympathomimetic drugs in aqueous solution. The electrochemical parameters of sympathomimetic drugs were investigated by means of cyclic voltammetry and differential pulse voltammetry as well as flow injection analysis.

Keywords: Zinc hydroxide, nanocrystal, sympathomimetic drugs, zinc compoundsh

1. Introduction

Because of their unusual physical and chemical properties compared to those of their bulk counterparts, nanomaterials have fascinated the scientific community in recent years. Nanoscale materials have potential applications as catalysts, drug delivery materials, photonic materials, and battery materials.[1,2] The morphology and size of the nanomaterials can greatly influence their optical, electronic, magnetic, and catalytic properties.[3,4] Much progress has been made on the size and morphology control of nanomaterials. Various materials with sizes in the range of several nanometers to micrometers were synthesized,[5] and a variety of morphologies such as nanotubes, nanowires, nanorings, ordered hexagonal mesostructures and nanorods have also been fabricated.[6–8] Due to its favorable structural, optical and catalytic properties, ZnO is often used in gas sensors, as antireflective coating and photocatalyst.[9–11]

The benefits of utilizing a solution-based method have also involved the considerable influence of reaction species on the final size and morphology of the as-prepared samples. Most of the previous works for the preparation of nano ZnO have used $Zn(OH)_2$ or its salts as a presubstance and water solvent as a media reaction. Further, systematic studies on the morphological modulation of ZnO, through using $Zn(OH)_4^{2-}$ or $Zn(NH_3)_4^{2+}$ as precursor, are still undeveloped. Therefore, it seems necessary to study the relationship between reaction conditions and ZnO morphologies for exploring an effective and simple route to control the morphology of ZnO nanostructures.[12,13] Different synthesis methods such as sol-gel technique, microemulsion synthesis, mechano-chemical processing, spray pyrolysis and drying, thermal decomposition, supercritical-water processing, self-assembling, hydrothermal processing, solvothermal vapor transport process, sonochemical or microwave-assisted synthesis, direct precipitation and homogeneous precipitation have been devised.[14–16]

In this paper, a new process for synthetizing $Zn(OH)_2$ and ZnO nanoparticles is presented. ZnO nanostructures were prepared by calcinating $Zn(OH)_2$ nanoparticles at 500 °C for 2 h. In the present work, ZnO nanostructures were found to be a highly active catalyst to-

wards the electrooxidation of some sympathomimetic drugs. Therefore, continuing our study in the preparation and use of nanocatalysts for the electrocatalytical oxidation and determination of important biological molecules,[17,18] we demonstrated the first application of ZnO nanocrystals for determination of electroactive sympathomimetic drugs in aqueous solutions by two electrochemical methods (Cyclic Voltametry (CV) and Differential Pulse voltametry (DPV)).

2. Experimental Section

2. 1. Materials and Methods

Zinc chloride ($ZnCl_2$) and ammonia solution (NH_4OH, 25.5%) were purchased from Merck Limited and used without further purification. Deionized water was used in experiments. All utilized chemicals used were of analytical grade. Solutions were prepared from analytical reagent grade chemicals without further purification. The phosphate buffer solution (PBS) (0.1 M) was prepared form H_3PO_4, KH_2PO_4 and K_2HPO_4. The pH of buffer solutions was adjusted with HCl and KOH solutions.

FTIR spectra were recorded using KBr disks on a Shimadzu FTIR model Prestige 21 spectrometer. The morphologies of products were observed with scanning electron microscopy (Philips XL-30). X-ray powder diffraction (XRD) measurements were performed using a Philips diffractometer manufactured by X'pert with monochromatized CuK_a radiation. The morphology and particle size were studied on a scanning electron microscope (SEM, LEO 1530 VP) and transmission electron microscope (TEM, JEM-100CX). EDX detector was used applying 15 kV accelerating voltage. Electrochemical measurements were carried out in a conventional three-electrode cell powered by an electrochemical system comprising an AUTOLAB system with PGSTAT12 boards (Eco Chemie, Utrecht, The Netherlands). The system was run on a PC using GPES 4.9 software. A saturated calomel electrode (SCE) was a reference electrode. All potentials were measured with respect to the SCE which was positioned as close to the working electrode as possible by means of a luggin capillary.

2. 2. Preparation of Nanostructures

In a typical experiment, 2 mmol $ZnCl_2$ $4H_2O$ was dissolved in 20 mL of deionized water in a 50 mL beaker. $NH_3(H_2O)$ (6 mol L^{-1}) was added dropwise under magnetic stirring. After formation of a white precipitate $NH_3(H_2O)$ was added continuously, and the precipitate was dissolved gradually. It was found that the color of the solution became clearer, which was indicative of $[Zn(NH_3)_4]^{2+}$ formation. When the pH of the solution was about 12, all of the precipitate was dissolved. The color of the solution turned into clear $[Zn(NH_3)_4]^{2+}$ 20 mL of concentrated sulfuric acid was poured into another beaker. Both beakers were covered with filter papers and were placed in a desiccator. Precipitate with a white color is formed gradually in left hand beaker (Scheme 1). Forty-eight hours later, the product was separated by centrifugation; washed three times using deionized water, and then dried in oven at 50 °C. The synthesis procedure is illustrated in Scheme 1.

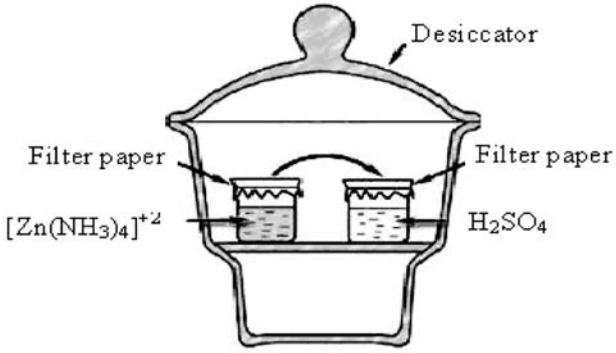

Scheme 1: Schematic representation of zinc hydroxide formation.

2. 3. Preparation of ZnO Modified Carbon Paste Electrode

Unmodified carbon paste electrode (UCPE) was prepared by hand-mixing carbon powder and mineral oil (Nojol), with the ratio of 60/40 (w/w %). The paste was carefully mixed and homogenized in an agate mortar for 25 min. The resulting paste was kept at room temperature in a desiccator. The paste was packed firmly into a cavity (3.6 mm diameter, geometric surface area of 0.1017 cm^2 and 0.5 mm depth) at the end of a Teflon tube. Electrical contact was established via a copper wire connected to the paste in the inner hole of the tube. The electrode surface was gently smoothed by rubbing on a piece of weighing paper just prior to use. This procedure was also used to regenerate the surface of the carbon paste electrodes. The ZnO nanoparticle-modified carbon paste electrodes (ZONM-CPEs) were prepared by mixing carbon powder together with ZnO nanoparticles at different ratios in an agate mortar until a uniform paste was obtained. The percentage (w/w) of zinc oxide informed throughout the text corresponds to the final percentage relative to the total paste composition. Then mineral oil was added (40 w/w %) and mixed thoroughly. The paste obtained was packed into a 3 mm diameter cavity at the end of a Teflon tube, and the electrical contact was provided with a copper wire.

3. Results and Discussion

3. 1. Characterization of $Zn(OH)_2$ and ZnO Nanostructures

The use of aqueous ammonia as the precipitator yields well-crystallized $Zn(OH)_2$ nanostructures. Fig. 1A

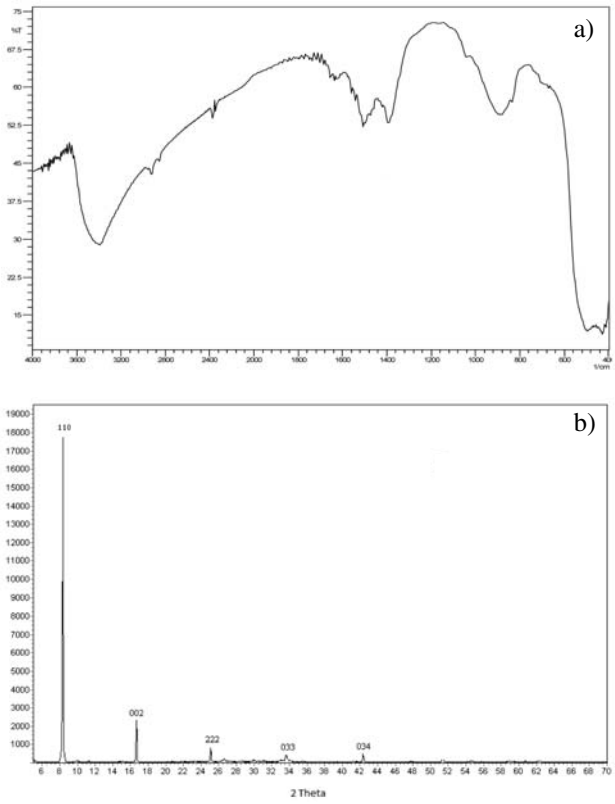

Fig. 1. (a) FT-infrared of $Zn(OH)_2$ nanostructures. **(b)** XRD patterns of $Zn(OH)_2$ nanostructures.

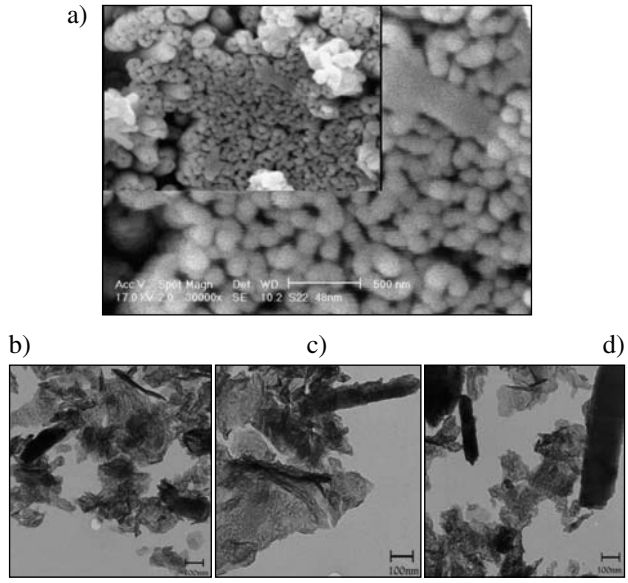

Fig. 2. (a) SEM image of the zinc hydroxide nanostructures, scale bar 48 nm. Inset: The SEM image with lower magnification for the same sample, scale bar is 1 μm, **(b–d)** TEM image of $Zn(OH)_2$ nanostructures.

shows the FTIR spectrum of the obtained $Zn(OH)_2$ nanocrystals. The strong broad absorption around 3400 cm^{-1} corresponds to the stretching of O–H from the hydroxyl groups.[19]

The peaks in the region of 1490–1300 cm^{-1} and 870 cm^{-1} can be assigned to hydroxyl group vibrations and in the region of 490–550 cm^{-1} can be assigned to metal-oxygen vibrations and metal-OH bending vibrations. Fig. 1B shows the XRD patterns of the $Zn(OH)_2$ nanocrystals. All the diffraction peaks can be indexed as the orthorhombic phase of pure $Zn(OH)_2$. The diffraction peaks in the XRD pattern can be readily indexed to crystalline bulk $Zn(OH)_2$. The lattice constants (a = 8.53 Å, b = 5.16 Å, c = 4.92 Å, Z = 4) calculated from this XRD pattern correspond well to the values given in the standard card (JCPDS 1–360). No impurity peaks are found, which implies a high purity of the as-synthesized $Zn(OH)_2$. The grain size of $Zn(OH)_2$ nanostructures is calculated by using the Scherer's equation:

$$D = \frac{0.9\lambda}{\beta \cos\theta} \tag{1}$$

where β is the broadening of diffraction line measured at half maximum intensity (radians) and λ = 1.54056 Å, the wavelength of the CuK X-ray. The grain size was found to be average 48 nm for $Zn(OH)_2$ nanostructures.

X-ray powder diffraction (XRD) patterns of the products were recorded at a scanning rate of 0.05°/s with 2θ range from 5 to 70°, with high-intensity CuK radiation (λ = 0.154178 nm). The grain size (D) estimated from the full width at half maximum of the dominant (110) peak at diffraction angle 2θ ~ 38.2°, using Scherrer's equation, was found to be ~48 nm.

The morphology of the precursor was investigated by SEM and TEM. The SEM micrograph in Fig. 2a shows the precursor consisted of a nanocrystal structures. Fig. 2(b-d) shows the TEM micrograph of the precursor, which is in nano scale.

There are several chemical reactions in the $[Zn(NH_3)_4]^{2+}$ solution. In the beginning, the $Zn(NH_3)_4^{2+}$ complex ions were very stable due to the relative high concentration of NH_3. Because it was a closed system, NH_3 would evaporate from the solution and can be absorbed by sulfuric acid in the other beaker. Equilibrium 2 was to the left side and some of the complex ions were dissociated gradually, so the concentration of hydrated zinc ions was increased. Due to evaporation, the concentration of NH_3 was decreased, and this made equilibrium 3 shift to the right side. The equilibrium reactions for equilibrium 2 and 3 are:

$$Zn^{2+} + 4NH_3 \leftrightarrow [Zn(NH_3)_4]^{2+} \tag{2}$$

$$[Zn(NH_3)_4]^{2+} + 2OH^- \leftrightarrow Zn(OH)_2 + 4NH_3 \tag{3}$$

Because the power of NH_3 concentration in the equation 2 is much higher than that of 3, the concentration decrease is much more important to equation 2 than for equation 3. Consequently, there is only a slight decrease of OH^- concentration. Due to the overall consideration of

the ion concentrations in the solution, the concentration of $[Zn^{2+}][OH^{-}]_2$ would increase. When this concentration product was greater than the solubility product of $Zn(OH)_2$ under the experimental conditions, the precursor of $Zn(OH)_2$ was formed.

Two possible growth mechanisms for the formation of these particles were proposed: the first was related to the stage of formation of nanorods from spherical colloids, and the second formation of wormlike particles from nanorods was described.

The as-prepared $Zn(OH)_2$ nanocrystals acting as a precursor, through dehydration, are converted into zinc oxide. This reaction can be schematized as follows:

$$Zn(OH)_2 \xrightarrow{dehydration} ZnO + H_2O \quad (4)$$

The product of the thermal decomposition from the $Zn(OH)_2$ nanocrystals was studied by FT-IR, XRD, and SEM, TEM. The FT-IR spectrum of the ZnO is shown at Fig. 3A. In the FT-IR spectra of the ZnO, absorption peaks at 3465 cm^{-1} are assigned to the stretching vibration of hydroxyl group and peaks around 504 and 443 cm^{-1} are ascribed to the ZnO stretching mode. Fig. 3B shows the XRD patterns of the dehydration product. All the reflection peaks can be indexed as pure hexagonal ZnO with cell parameters a = 3.248 A° and c = 5.206 A°, which are in agreement with the literature values (JCPDS card number 3–888). The diffraction peaks are well broadened, and analysis of the peak broadening with the Debye-Scherr equation shows the average crystal domain size to be 69 nm. No impurity peaks are found, suggesting a high purity of the as-synthesized ZnO nanostructures. Thus, the as-prepared ZnO has a pure single phase of hexagonal wurtzite structure. For further demonstration, the EDAX was performed for the ZnO nanostructures. EDAX spectrum is shown in Fig. 3C which is indicative of convenient and suitable purity of ZnO nanostructures.

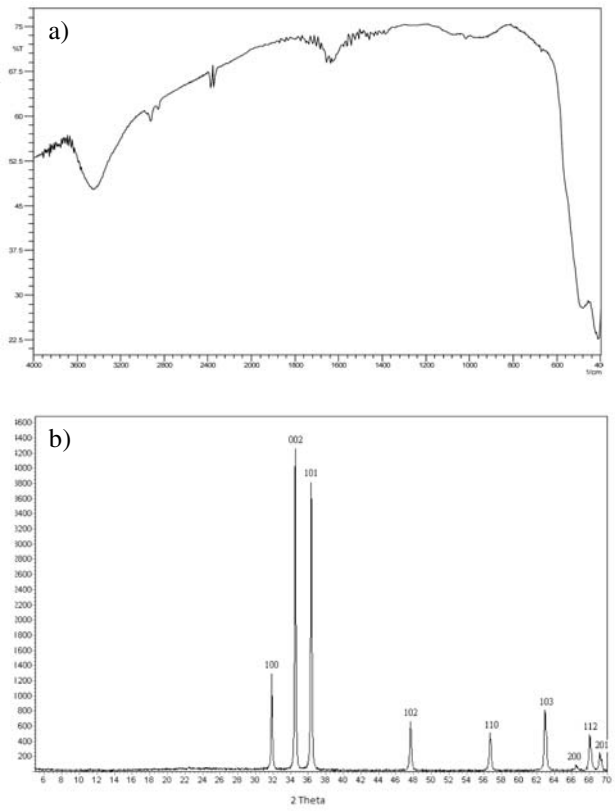

Fig. 3. (a) FTIR spectra ZnO nanostructures after calcinations. **(b)** XRD patterns and EDX patterns of ZnO nanostructures **(c)**.

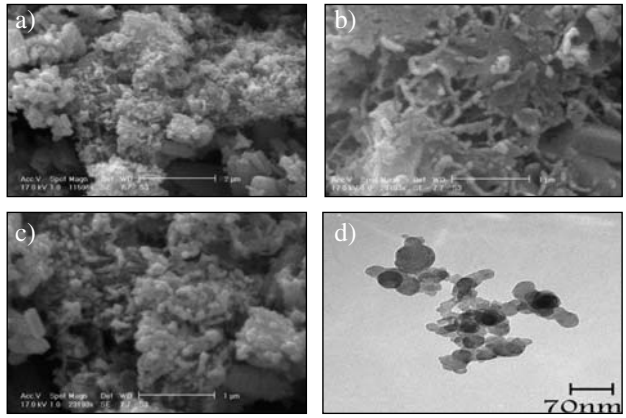

Fig. 4. (a,b,c) SEM image of rod-like ZnO nanostructures, **(d)** TEM image of rod-like ZnO nanostructures.

AFigs. 4 a–c show the SEM micrograph of ZnO after calcination, which is composed of nanoparticles. Fig. 4d shows the TEM image of ZnO nanoparticles which confirmed obtained results from SEM.

3. 2. Electrocatalytic Oxidation and Determination of Sympathomimetic Drugs using ZNOM-CPEs

In the area of electrochemical sensors, the special properties of ZnO nanoparticles have gradually attracted much attention.[20,21] For example, Zhang *et al.,*[20] developed a new electrochemical sensor based on ZnO to detect ion of uric acid.

This study was aimed at the surfactant-free method preparation of ZnO nanoparticles. Following, ZnO nanoparticles were applied for selective determination of sympathomimetic drugs. Its nice biocompatibility and fast electron transfer ability have made the material able to function as a new electrochemical modifier for the preparation of sympathomimetic drugs sensors.

ZnO nanoparticles have been used for electrocatalytic oxidation and determination of sympathomimetic drugs in aqueous solution. The electrocatalytic activity of ZNOM-CPEs was examined by cyclic voltammetry. Fig. 5A shows the cyclic voltammograms responses of 0.62 mM methylephedrine at the bare CPE and ZNOM-CPEs in (pH 7.2) at scan rate 100 mVs^{-1}. The modified electrode exhibits significant oxidation currents starting around 0.6 V *vs.* SCE and a reduction signal around 0.37 V is observed in the reversed scan. In contrast low redox activity is observed at the unmodified carbon paste electrode (CPE) over the same potential range. A substantial negative shift of the anodic peak potential and dramatic increase of current indicate significant catalytic ability of ZNOM-CPES to methylephedrine oxidation. Due to high specific area of ZNOM-CPES, methylephedrine more easily penetrates through the conductive porous channels of the electrode, leading to higher sensitivity. The reproducibility of ZNOM-CPEs for catalytic oxidation of methylephedrine is evaluated by five independently prepared modified electrodes. Cyclic voltammograms (CV) are recorded in 0.62 mM methylephedrine solution (RSD was 3.2%). The relative standard deviation (RSD) of the peak currents of 0.62 mM methylephedrine for eight repeated determinations is also 3.0%. Then at the surface of ZNOM-MCPEs not only the over-voltage for methylephedrine oxidation decreased but also the antifouling properties of modified film improved reproducibility. CV of 0.62 mM methylephedrine solution at different scan rates was recorded (not shown). The peak current for the anodic oxidation of methylephedrine is proportional to the square root of scan rate, which is the ideal case for quantitative applications. In order to optimize the electrocatalytic response of modified electrodes toward methylephedrine oxidation the effect of pH on the catalytic oxidation behavior was investigated. The differential pulse voltametry (DPV) of ZNOM-MCPEs in 7 µ1M methylephedrine at different pH values (2–11) were recorded (not shown). With increasing pH values the potential of methylephedrine oxidation peak shifts to less positive value and the current peak is almost unchanged. Since more reproducible results and high catalytic activity of modified electrode are observed at pH 6–10, the methylephedrine measurement was done at pH value 7.2. The DPV of modified electrode in the presence of different concentration of methylephedrine, 0.09–0.7 mM was recorded (Fig. 5B). A linear dependence of the catalytic currents *vs.* concentration of methylephedrine can be fitted in the equation:

$$I\ (nA) = 400.1\ [methylephedrine]\ nA\ \mu 1M^{-1} + 23.5\ nA \text{ and } R^2 = 0.9927.$$

The detection limit was 0.01 mM at signal to noise ratio of 3 (Fig. 5C). Similar DPV curves were collected for ephedrine and norephedrine. The detection limit (LOD), quantization limit (LOQ), and linear range (mM), values were obtained according to DPV technique for these sympathomimetic drugs The oxidation process of the ZNOM-CPEs exhibited similar electrocatalytic responses for other sympathomimetic drugs, thus demonstrating its capability for selective oxidation of sympathomimetic drugs.

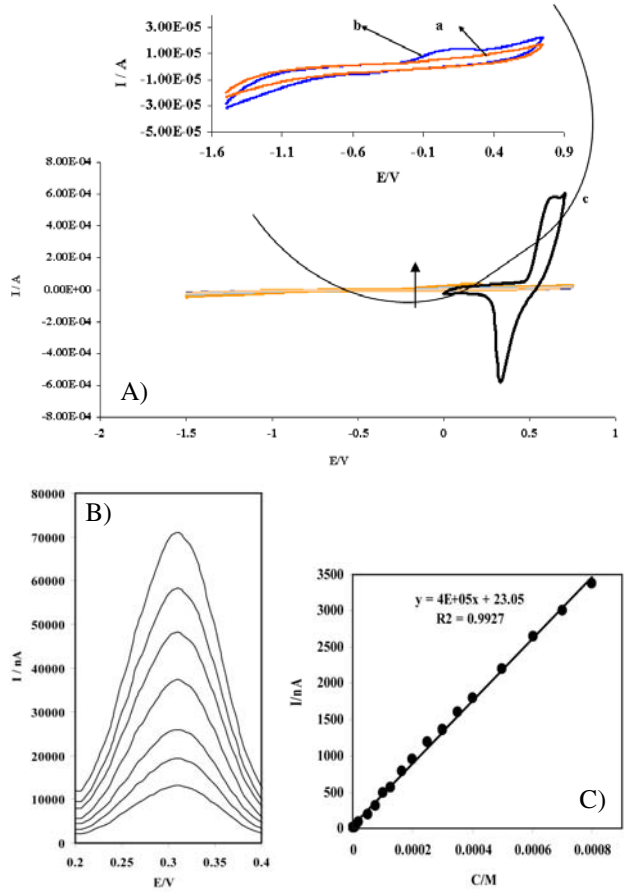

Fig. 5. A) Cyclic voltammograms of ZON-MCPEs in pH 7.2 solution at scan rate 100 mV s–1 in the absence (b) and presence 0.62 mM methylephedrine (c). (a) as (b) is cyclic voltammogram for bare carbon paste electrode. Inset is magnified CV of Fig. 5A. B) DPV of ZNOM-CPEs in pH 7.2 buffer containing different concentration of methylephedrine, 0.09, 0.97, 0.1, 0.3, 0.5, 0.6 and 0.7 mM. C) Plot of peak current vs. methylephedrine concentration.

3. 2. 2. Flow Injection Analysis of Methylephedrine at ZNOM-CPEs

The amperometry under stirred conditions or the flow injection analysis with amperometric detection is employed for low concentration analysis. Flow injection analysis of methylephedrine is used for assessing the tem-

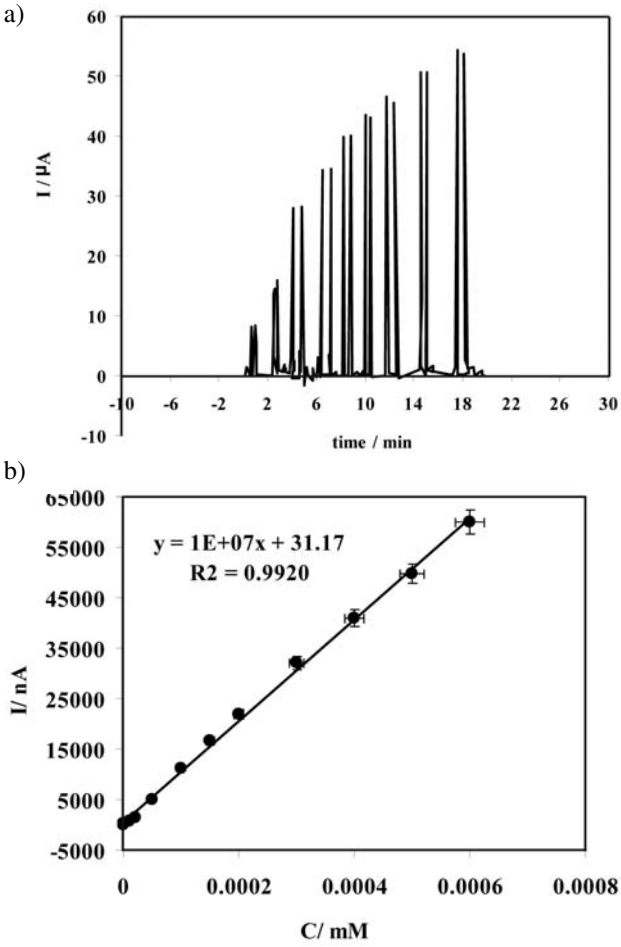

Fig. 6. (a) FIA responses to 0.9, 1, 1.5, 1.8, 2.4, 3.1, 4.2, 6 and 8 µM methylephedrine, operation potential 0.6 V. Carrier was phosphate buffer solution (pH 7.2). **(b)** The resulting calibration plot.

poral response and overall analytical performance of the sensor. The subsequent flow injection experiments were performed using the pH 7.2 phosphate buffer as a carrier solution and 0.6 V as a sensing potential. Fig. 6 compares the amperometric response of the sensor to successive additions of 0.22 µ1M methylephedrine. Alternative injections produce reproducible amperometric response signals, indicating no memory effect and surface fouling occurred during the successive measurements of methylephedrine. As indicated from the resulting calibration plot (inset), the response of the modified electrode is linear over the entire 0.9–8 µ1M, and concentration range with correlation coefficient of 0.9920. The favorable signal to noise characteristics of these data indicates a detection limit of 0.07 µ1M. similar results were obtained for ephedrine and norephedrine. The values of analytical parameters according to the flow injection analysis reported in Table 1.

4. Conclusions

To sum up, $Zn(OH)_2$ nanocrystals with hexagonal structure have been synthesized by means of a novel and simple one-step method from $[Zn(NH_3)_4]^{2+}$ precursor. The synthesized $Zn(OH)_2$ nano-worms acting as a precursor are further converted into zinc oxide nanoparticles through dehydration. Also, we have presented electrochemical application of ZnO nanoparticles. The electrooxidation of sympathomimetic drugs was successfully performed using the ZnO modified carbon past electrode. The modified electrode shows excellent electrocatalytic activity for sympathomimetic drugs oxidation. The analytical performance of modified electrode indicates that it can be used as sensitive amperometric detector for micromolar detection of sympathomimetic drugs when coupled with flow system.

5. Acknowledgments

We are grateful to Payame Noor University and Drug Applied Research Center, Tabriz University of Medical Sciences for financial support of this work.

6. References

1. Z. Q. Li, Y. Ding, Y. J. Xiong, Q. Yang, Y. Xie, *Chem. Commun.* **2005**, *7*, 918–920.
2. A. D. Dinsmore, M. F. Hsu, M. G. Nikolaides, M. Marquez, A. R. Bausch, D. A. Weitz, *Science* **2002**, *298* , 1006–1009.
3. V. I. Klimov, R. V Annu, *J. Phys. Chem.* **2007,** *58*, 635–673.
4. L. Li, J. Hu, W. Yang, A. P. Alivisatos, *Nano Lett.* **2001,** *1*, 349–351.
5. D. Y. Han, H. Y. Yang, C. B. Shen, X. Zhou, F. H. Wang, *Powder Technol.* **2004**, *147*, 113–116.

Table 1. Results obtained from sympathomimetic drugs analysis in buffer solution (pH = 7.2)

Method	Sympathomimetic Drugs	Dynamic range/	LOD	LOQ	RSD (%)
DPV	methylephedrine	0.08–0.8 mM	0.03 mM	0.09 mM	3.2
	ephedrine	0.2–18 mM	0.08 mM	0.19 mM	2.01
	norephedrine	20–700 mM	16 mM	37.20 mM	3.00
FIA	methylephedrine	0.04–1 µ1M	0.07 µ1M	0.117 µ1M	1.82
	ephedrine	0.9–1200 µ1M	0.62 µ1M	2.10 µ1M	1.30
	norephedrine	65–1000 µ1M	31.04 µ1M	73.00 µ1M	2.14

6. H. J. Liu, T. Y. Peng, D. E. Zhao, K. Dai, Z. H. Peng, *Mater. Chem. Phys.* **2004**, *87*, 81–86.
7. O. Yang, J. Sha, X. Y. Ma, D. R. Yang, *Mater. Lett.* **2005,** *59*, 1967–1670.
8. B. Zhao, X. K. Ke, J. H. Bao, C.L. Wang, L. Dong, Y. W. Chen, H. L. Chen, *J. Phys. Chem.* **2009,** *113*, 14440–14447.
9. J. G. Lu, P. Chang, Z. Fan, *Mater. Sci. Eng.* R. **2006**, *52*, 49–91.
10. X. Cao, N. Wang, L. Wang, L. Guo, *J .Nanopart. Res.* **2010,** *12*, 143–150.
11. H. Chen, X. Wu, L. Gong, C. Ye, F. Qu, G. Shen, *Nanoscale Res. Lett.* **2010**, *5*, 570–575.
12. J. Zhang, L. Sun, J. Yin, H. Su, C. Liao, C. Yan, *Chem. Mater.* **2002,** *14*, 4172–4177.
13. Y. Li, B. Tan, Y. Wu, *Chem. Mater.* **2008,** *20*, 567–576.
14. S. Ashoka, P. Chithaiah, K. V. Thipperudraiah, G. T. Chandrappa, *Inorg. Chim. Acta* **2010**, *363*, 3442–3447.
15. B. I. Kharisov, O. V. Kharissova, M. J. Yacaman, *Ind. Eng. Chem. Res.* **2010**, *49* 8289–8309.
16. Z. Yang, Q. H. Liu, *Physica E.* **2008**, *40*, 531–535.
17. M. Hasanzadeh, G. Karim-Nezhad, N. Shadjou, M. Hajjizadeh, B. Khalilzadeh, L. A. Saghatforoush, M. H. Abnosi, A. Babaei, S. Ershad, *Anal. Biochem.* **2009**, *389*, 130–137.
18. M. Hasanzadeh, N. Shadjou, L. A. Saghatforoush, R. Mehdizadeh, S. Sanati, *Catal. Commun.* **2012**, *19*, 10–16.
19. M. C. Neves, T. Trindade, A. M. B. Timmons, J. D. Pedrosa de Jesus, *Mater. Res. Bull.* **2001,** *36*, 1099–1108.
20. F. Zhang, X. Wang, S. Sun, Z. Wan, Q. Zhu, Z. Xian, Y. Jin, L. Yamamoto, *Anal. Chim. Acta* **2004**, *519*, 155–160.
21. T. Yumak, F. Kuralay, M. Muti, A. Sinag, A. Erdem, S. Abaci, Colloid Surface B. **2011**, *86*, 397–403.

Povzetek

Z uporabo dvostopenjske metode brez kalupa in brez surfaktanta smo uspešno sintetizirali nanodelce cinkovega hidroksida ($Zn(OH)_2$) z nanokristalinično morfologijo in velikostjo zrn 48 nm. Sintetizirani produkt smo okarakterizirali s FTIR, praškovno X-žarkovno difrakcijo (XRD), vrstično elektronsko mikroskopijo (SEM), transmisijsko elektronsko mikroskopijo (TEM) in disperzijsko X-žarkovno spektroskopijo (EDX). XRD spekter cinkovega oksida potrjuje nastanek wurtzitne strukture $Zn(OH)_2$. Prvič smo uporabili nanostrukture cinkovega oksida za elektrokatalitsko oksidacijo in določitev simpatomimetičnih učinkovin v vodni raztopini. Elektrokemične parametre simpatomimetičnih učinkovin smo raziskovali s ciklično voltametrijo in diferenčno pulzno voltametrijo ter s pretočno analizo (FIA).